6540 *Biochemistry* **2009,** *48,* 6540–6550
DOI: 10.1021/bi900181w

BIOCHEMISTRY
including biophysical chemistry & molecular biology
Article

IgE Receptor-Mediated Alteration of Membrane−Cytoskeleton Interactions Revealed by Mass Spectrometric Analysis of Detergent-Resistant Membranes[†]

Xuemei Han,[‡] Norah L. Smith,[‡] Dwaipayan Sil, David A. Holowka, Fred W. McLafferty, and Barbara A. Baird*

Department of Chemistry and Chemical Biology, Cornell University, Ithaca, New York 14853-1301 [‡]*These authors contributed equally to this work*

Received February 4, 2009; Revised Manuscript Received June 3, 2009

ABSTRACT: We use electrospray ionization mass spectrometry to quantify >100 phospholipid (PL) components in detergent-resistant membrane (DRM) domains that are related to ordered membrane compartments commonly known as lipid rafts. We previously compared PL compositions of DRMs with plasma membrane vesicles and whole cell lipid extracts from RBL mast cells, and we made the initial observation that antigen stimulation of IgE receptors (FcεRI) causes a significant change in the PL composition of DRMs [Fridriksson, E. K., et al. (1999) *Biochemistry 38*, 8056−8063]. We now characterize the signaling requirements and time course for this change, which is manifested as an increase in the recovery of polyunsaturated PL in DRM, particularly in phosphatidylinositol species. We find that this change is largely independent of tyrosine phosphorylation, stimulated by engagement of FcεRI, and can be activated by Ca^{2+} ionophore in a manner independent of antigen stimulation. Unexpectedly, we found that inhibitors of actin polymerization (cytochalasin D and latrunculin A) cause a similar, but more rapid, change in the PL composition of DRMs in the absence of FcεRI activation, indicating that perturbations in the actin cytoskeleton affect the organization of plasma membrane domains. Consistent with this interpretation, a membrane-permeable stabilizer of F-actin, jasplakinolide, prevents antigen-stimulated changes in DRM PL composition. These results are confirmed by a detailed analysis of multiple experiments, showing that receptor and cytochalasin D-stimulated changes in DRM lipid composition follow first-order kinetics. Analysis in terms of the number of double bonds in the fatty acid chains is valid for total PL of the major headgroups and for headgroups individually. In this manner, we show that, on average, concentrations of saturated or monounsaturated PL decrease in the DRM, whereas concentrations of PL with two or more double bonds (polyunsaturated PL) increase due to cytoskeletal perturbation. We find that these changes are independent of fatty acid chain length. Our mass spectrometric analyses provide a detailed accounting of receptor-activated alterations in the plasma membrane that are regulated by the actin cytoskeleton.

Functional roles for lipid heterogeneity and lipid-based membrane domains in cellular processes have received increasing amounts of attention over the past decade (*1*, *2*). Central to this topic are regions of the plasma membrane containing lipids with liquid-ordered-like phase behavior, commonly called lipid rafts (*2*, *3*). Originally identified as a subset of plasma membrane lipids and proteins that are not solubilized by mild detergents such as Triton X-100 (*4*−*6*), these membrane domains have been implicated in a variety of cellular functions, including receptor signaling, vesicle trafficking to and from the plasma membrane, and host−pathogen interactions (*7*−*9*). Studies on model membranes show that membrane domains composed predominately of cholesterol and sphingomyelin or saturated phosphoglycerolipids are in an Lo[1] phase that is sufficient to confer detergent resistance and segregation from liquid-disordered (Ld) regions of lipid bilayers (*2*). However, because lipid rafts in cells have variable lipid and protein composition, are dynamic, and are difficult to detect by optical microscopy or other nondestructive methods, their true nature and even their existence in live cells have been subjects of controversy (*10*, *11*) and continue to be evaluated with the development of new approaches (*12*, *13*).

Although use of detergent resistance as an indicator for lipid rafts in cells requires careful interpretation, this property continues to serve as a valuable correlative tool (*13*). A complementary approach frequently used to visualize coalesced lipid rafts in live cells is to cross-link certain receptors or lipid raft components under conditions that result in large-scale coclustering of other raft components (*14*−*17*). Results from these fluorescence imaging experiments are generally consistent with predictions

[†]This research was supported by National Institutes of Health Grants AI018306 (B.A.B. and D.A.H.) and GM016609 (F.W.M.) and in part by the Nanobiotechnology Center (NSF-ECS-9876771).

*To whom correspondence should be addressed. Phone: (607) 255-4095. Fax: (607) 255-4137. E-mail: bab13@cornell.edu.

[1]Abbreviations: DRM, detergent-resistant membrane; PL, phospholipid; FTMS, Fourier transform mass spectrometry; BSS, buffered saline solution; ESI-MS, electrospray ionization mass spectrometry; P/(S+M), polyunsaturated PL/(saturated PL + monounsaturated PL); db, double bond; Lo, liquid-ordered; Ld, liquid-disordered.

 Published on Web 06/04/2009 © 2009 American Chemical Society

from detergent-dependent membrane fractionation (*8*, *12*), and used together with biological assays, they support the relevance of this biochemical approach to the functional characterization of lipid rafts and associated components. In mast cells, cross-linking of the high-affinity IgE receptor, FcεRI, causes its stable association with lipid rafts as assessed by cell lysis with low concentrations of detergent (e.g., 0.05% Triton X-100) and sucrose gradient fractionation. This association is highly correlated with the initiation of cell signaling mediated by native FcεRI (*18*) or chimeric, single-chain IgE receptors (*19*).

Under experimental conditions that show co-redistribution of lipid raft components at the cell surface, F-actin is commonly found to colocalize with raft domains by fluorescence microscopy imaging, suggesting a structural relationship between lipid rafts and the cortical cytoskeleton (*20*−*22*). Consistent with this observation, alteration of cholesterol content that inhibits initiation of IgE receptor signaling (*16*) can also perturb plasma membrane−cytoskeleton interactions (*23*). Results in this study provide new evidence from mass spectrometry of significant coupling between lipid rafts and the actin cytoskeleton.

In a previous study (*24*), we used Fourier transform mass spectrometry (FTMS) with electrospray ionization (ESI-MS) to characterize the phospholipid (PL) composition of plasma membranes and detergent-resistant membranes (DRMs) isolated from RBL mast cells. The unusual FTMS capabilities of resolving power and sensitivity identified unique molecular masses of nearly 100 components, including a number of new species, while mass isolation and dissociation of individual molecular ions provided fragment masses for reliable molecular characterization (*24*). We showed that both of these membrane preparations are enriched in sphingomyelin and phosphoglycerolipids with saturated or monounsaturated acyl chains, compared to phosphoglycerolipids with polyunsaturated acyl chains. However, the DRM preparations have significantly higher percentages of sphingomyelin and saturated acyl chains, as expected for Lo domains. In contrast, PLs extracted from the whole cells are highly enriched in polyunsaturated species. We discovered that stimulation of RBL cells via FcεRI causes a substantial increase in the ratio of polyunsaturated to saturated plus monounsaturated PLs [P/(S+M)] recovered in DRMs. The structural and functional basis for this stimulated change was intriguing but unclear. In this study, we collect and analyze extensive mass spectrometry data to characterize this DRM lipid compositional change and its temporal trend, and we find that this change follows first-order kinetics and depends on stimulated changes in the actin cytoskeleton. Our results point to sensitive, dynamic regulation of lipid rafts by the actin cytoskeleton that is modulated during receptor-mediated cell activation.

MATERIALS AND METHODS

Cell Stimulation, DRM Vesicle Isolation, and Lipid Extraction. Methods used are similar to those described by Fridriksson et al. (*24*), with some modifications. RBL-2H3 cells (*25*) were sensitized overnight with a 2−5-fold molar excess over FcεRI of purified anti-DNP IgE (*26*). Cells were harvested, washed twice with buffered saline solution (BSS) [135 mM NaCl, 5 mM KCl, 1 mM $MgCl_2$, 1.8 mM $CaCl_2$, 5.6 mM glucose, 20 mM HEPES (pH 7.4), and 1 mg/mL BSA], and resuspended at a density of 8×10^6 cells/mL. Cells were stimulated with multivalent DNP-BSA (2−5 μg/mL) for 2−30 min at 37 °C. For some experiments, the Src family tyrosine kinase inhibitor PP1 (BioMol, Plymouth Meeting, PA) was added at a concentration 4 μM, 2 min prior to antigen stimulation. For other experiments, jasplakinolide (Invitrogen/Molecular Probes, Eugene, OR) was added at a concentration of 3 μM for 1 h at 37 °C prior to antigen stimulation. Alternatively, cells were stimulated with 0.9 μM A23187 (Calbiochem, San Diego, CA) for 5 or 15 min or treated with 0.2−2 μM cytochalasin D (Sigma Chemical Co., St. Louis, MO) or 0.2 μM latrunculin A (Invitrogen/Molecular Probes) for 1, 2, or 10 min, all at 37 °C.

Following stimulation, we lysed cells by mixing them in a 1:1 ratio with 2× ice-cold lysis buffer (20 mM Tris-HCl, 100 mM NaCl, 2 mM sodium orthovanadate, 60 mM sodium pyrophosphate, 20 mM sodium glycerophosphate, 0.04 unit/mL aprotinin, and 0.02% sodium azide) containing 0.09% Triton X-100 and 2 mM 4-(2-aminoethyl)benzenesulfonyl fluoride hydrochloride (AEBSF) (Sigma). After 10 min at 4 °C, 3.6 pmol of 1,2-dinonadecanoyl-*sn*-glycero-3-phosphatidylcholine (Avanti; PC 38:0) was added as an exogenous lipid standard (accounts for 1−2 mol % of total lipids detected). Then 10 mL of this cell lysate was mixed in a 1:1 ratio with 80% sucrose (w/v) in HEPES/saline buffer [25 mM HEPES, 150 mM NaCl, and 2 mM EDTA (pH 7.5)]. These lysates were placed in centrifuge tubes, and then 5 mL of 35% sucrose and 5 mL of 5% sucrose in HEPES/saline buffer were carefully layered on top of the 40% sucrose solution containing the cell lysates. Gradients were centrifuged at 100000*g* for 15−18 h at 4 °C using a Beckman SW-28 rotor in a Sorvall Discovery 100S ultracentrifuge.

After centrifugation, two opaque bands were visible, and the upper band (3 mL), previously identified as that containing the DRMs (*24*), was collected from the interface of the 5 and 35% layers. The contents were diluted with 15 mL of phosphate-buffered saline (PBS) containing 1 mM EDTA and centrifuged at 300000*g* for 30 min at 4 °C in a Beckman Ti60 rotor. Pellets were resuspended in 400 μL of a PBS/EDTA mixture, and lipids were extracted using a modified Bligh−Dyer method (*27*): the suspended pellets were each mixed with 1.5 mL of a chloroform/methanol mixture at a 1:2 ratio and vortexed, then 0.5 mL of chloroform was added, and samples were vortexed again. Finally, 0.5 mL of 2 N HCl was added, and samples were vortexed and then centrifuged at 2000*g* for 5 min to achieve phase separation. The lower (chloroform) layer was collected and used for ESI-MS analysis. To determine the plasmalogen content of DRMs, pellets were resuspended in 400 μL of 50 mM LiCl (pH 6); 50 mM LiCl was also used in place of 2 N HCl in the extraction process (*28*).

To determine the percentage of cellular PL recovered in DRMs, 2×10^6 cells in BSS were pelleted and resuspended in 400 μL of a PBS/EDTA mixture, and PLs were extracted as described for DRMs. For organic phosphate analysis to quantify PL concentrations, extracted PL in chloroform from either DRMs (200 μL) or cells (1 mL) was treated as described previously (*58*), and the amount of organic phosphate was used as a measure of PL recovered. Comparison of PL recovered per cell equivalent of extracted DRMs and cells permits calculation of the percentage of PL recovered in DRMs.

Tyrosine Phosphorylation Assay. RBL-2H3 cells were sensitized overnight with IgE as described above, harvested and washed twice with BSS, and then resuspended at a density of 2×10^6 cells/mL. Cells were then stimulated with DNP-BSA (0.8 μg/mL) in the presence or absence of 4 μM PP1 at 37 °C for the times indicated. Samples were quenched by addition of 5× sample buffer [50% glycerol, 0.25 M Tris (pH 6.8), 5% (w/v)

SDS, and 0.05% (w/v) bromophenol blue] and boiling for 5 min. Samples were electrophoresed and detected by Western blotting with 4G10 anti-phosphotyrosine (*19*).

Cholesterol Content Assay. Free cholesterol in DRMs was assayed using the Amplex Red Cholesterol Assay Kit (Invitrogen/Molecular Probes) following kit instructions, except that cholesterol esterase was omitted from the DRM samples. Following specified incubations, samples were placed on ice, and sample fluorescence was measured with an SLM 8000C spectrofluorometer. We found that 10 μL aliquots of pelleted, resuspended DRMs contain cholesterol values in the linear region of the standard curve.

Quantitative Analysis of Phospholipids Using Electrospray Ionization Mass Spectrometry (ESI-MS). Spectra were acquired on a modified 6T Finnigan (Madison, WI) FTMS instrument equipped with an electrospray ion source, as described previously (*29*). Prior to nanospraying, we diluted lipid extracts prepared as described above 10-fold in a 49:49:2 (v/v/v) methanol/chloroform/acetic acid mixture for the positive ion mode and 10-fold in a 1:1 (v/v) methanol/chloroform mixture for the negative ion mode (*30*, *31*). Typically, fewer than 2×10^5 cell equivalents of the lipid extract (<6 nmol of phospholipid) were needed to obtain complete positive and negative mode spectra. For identification of plasmalogen species in the extract, LiOH was added to a final concentration of 2 mM prior to the analyses; in the positive ion spectra, the lipid species were observed as Li adducts (+6 Da). For each sample, four separate aliquots were measured, and mole percentage (mol %) values (±standard deviation) were determined for each species.

Relative instrument responses (peak intensity per mole of analyte) were determined using a standard mixture of phosphatidylcholine (PC), phosphatidylethanolamine (PE), sphingomyelin (SM), phosphatidylinositol (PI), phosphatidylglycerol (PG), phosphatidylserine (PS), and phosphatidic acid (PA) at equimolar ratios for both the positive ion mode and the negative ion mode (*24*). The variation of instrument response per mole with acyl chain length and degree of unsaturation was not evaluated, but it is far smaller than that with headgroups at the low concentration used here (*32*). Any such variation will not affect the change in the mol % values with experimental parameters on a relative basis. As previously established (*33*), below 100 μmol of total lipids, there are no aggregated ions, and the ion counts are proportional to lipid concentrations in these limits. The detailed ESI-MS data were tabulated as mol % values for each PL headgroup in terms of acyl chain length (number of carbon atoms) and number of double bonds (see Table 1). For kinetic analyses, these values are summed for both acyl chains of PC, PE, PS, PI, PG, and PA or for the single acyl chain of SM. The mol % data were compiled for samples taken at multiple time points after initiation of a specified treatment. Table 1 and Figures 3 and 5 show representative data from a single experiment. Figures 1, 2, and 4 show data from multiple experiments averaged together.

Kinetic Analysis of PL Changes. For systematic analysis over multiple samples and experiments with different treatments, the PL composition data are compared in terms of headgroups, the total number of double bonds in the acyl chains (db0, db1, db2, db3, and db4+), and acyl chain length. A simple evaluation of time-dependent changes monitors acyl chain saturation and represents the mol % abundance data as the lumped ratio P/(S+M), where P corresponds to polyunsaturated (db2, db3, and db4+) acyl chains, S corresponds to saturated (db0) acyl chains, and M corresponds to monounsaturated (db1) acyl chains (see Figure 2).

For a comprehensive analysis of compositional changes with time, the mol % values are evaluated with a first-order kinetic model. Useful parameters for comparison are the value of first-order rate constant k together with the direction and magnitude of the concentration change. We consider a species with concentration $C(t)$ that may increase or decrease with time after stimulation; C_i corresponds to the initial (prestimulation) concentration, and C_f corresponds to the final concentration that stabilizes after stimulation.

$$[C(t)-C_f]/(C_i-C_f) = \exp(-kt)$$

$$C(t) = (C_i-C_f)\exp(-kt)+C_f \quad (1)$$

For species with decreasing concentrations, $C_i-C_f>0$, and for species with increasing concentrations, $C_i-C_f<0$. The direction of the change is given by the value $n=(C_f-C_i)/|C_f-C_i|$. Because of the absolute value in the denominator, $n=-1$ for species that undergo a decrease in concentration and $n=1$ for species that undergo an increase in concentration. The lumped term $k_m=nk$ represents the value of the rate constant and the direction of concentration change.

For sufficiently short times, as compared to the time course of the concentration change, the exponential in eq 1 can be replaced by a truncated Taylor series, $\exp(-kt)\simeq 1-kt$, yielding a linear expression for $C(t)$ versus t and an approximate first-order rate constant k_a:

$$C(t) = C_i+(C_f-C_i)k_a t \quad (2)$$

Note that the slope in this linear approximation $k_s=(C_f-C_i)k_a$ is a lumped term representing the magnitude and direction of the concentration change times the value of k_a. The mol % $[C(t)]$ data are plotted according eq 1 (Figure 1A,B) or eq 2 (Figure 3). From these primary plots, the values of $k_m=nk$ (Figure 1C) or $k_s=(C_f-C_i)k_a$ (Figures 4 and 5) are plotted as a function of the total number of double bonds in the acyl chains with specified headgroups.

Data fitting for exponential curves over longer time periods (eq 1, Figure 1A,B) and linear approximation curves at short times (eq 2, Figure 3) was conducted with MATLAB. We determined the linear approximation to be valid for DNP-BSA stimulation by the following comparison. Using mol % at long times (C_f) obtained from fitting the data in Figure 1A with eq 1, the value for C_f-C_i was determined, and the approximate rate constant k_a was calculated from $(C_f-C_i)k_a$ values obtained from the linear fit (eq 2, Figure 3). We find that these k_a values are very similar to k values obtained directly from Figure 1A. Similarly, from a linear fit (eq 2) of the 0, 2, 5, and 10 min data of Figure 1A, the slope $(C_f-C_i)k$ values were determined. These are also very similar to the $(C_f-C_i)k_a$ values obtained from the slopes in Figure 3. This validation of the linear approximation for DNP-BSA stimulation allowed direct comparison of multiple treatments over the shorter time period (Figure 4).

RESULTS

Unsaturated PL Increase in DRM Fractions upon Receptor-Mediated Cell Activation. A complete PL analysis was conducted by ESI-MS for DRM samples from cells before and after stimulation with the antigen DNP-BSA at several time points, as represented by the experiment given in Table 1.

Table 1: Normalized Mole Percentages of PL in DRMs Isolated from Cells before and at Specified Times after DNP-BSA Stimulation

	PC $(M+H)^+$				SM $(M+H)^+$				PE $(M+H)^+$				PS $(M-H)^-$				PI $(M-H)^-$				PG $(M-H)^-$				PA $(M-H)^-$			
lipid[a]	0[b]	2[b]	5[b]	10[b]	0[b]	2[b]	5[b]	10[b]	0[b]	2[b]	5[b]	10[b]	0[b]	2[b]	5[b]	10[b]	0[b]	2[b]	5[b]	10[b]	0[b]	2[b]	5[b]	10[b]	0[b]	2[b]	5[b]	10[b]
32:0	1.2	0.6	0.6	0.4																	0.01	0.02	0.02	0.01				
34:0	1.2	0.9	0.7	0.5					1.7	0.9	1.0	0.8	0.1	0.1	0.2	0.2	0.2	0.4	0.3	0.4	0.05	0.07	0.07	0.09				
36:0	0.4	0.3	0.2	0.2					1.8	1.2	1.2	0.8	0.8	0.7	0.6	0.6	0.9	0.6	1.3	1.1	0.04	0.03	0.06	0.05	0.02	0.04	0.03	0.04
40:0									0.7	0.6	0.5	0.9																
16:0					3.6	4.0	3.4	1.8																				
18:0					5.3	4.0	3.4	2.0																				
24:0					8.7	7.4	5.6	3.2																				
sum S	**2.8**	**1.8**	**1.5**	**1.1**	**17.7**	**15.3**	**12.4**	**7.1**	**4.2**	**2.8**	**2.7**	**2.6**	**0.9**	**0.9**	**0.8**	**0.8**	**1.1**	**0.9**	**1.5**	**1.5**	**0.09**	**0.11**	**0.14**	**0.15**	**0.02**	**0.04**	**0.03**	**0.04**
SD	0.3	0.2	0.2	0.3	0.7	2.2	1.7	0.7	1.2	0.4	0.3	0.6	0.0	0.2	0.3	0.1	0.0	0.2	0.8	0.5	0.02	0.03	0.05	0.02	0.00	0.01	0.01	0.03
32:1	1.0	0.6	0.6	0.4																	0.01	0.01	0.01	0.02	0.02	0.04		
34:1	4.7	3.9	3.1	2.1					1.1	0.8	0.8	0.8	0.5	0.8	0.6	0.8	0.7	1.3	1.1	1.8	0.25	0.41	0.34	0.50	0.05	0.10		
36:1	2.8	2.2	1.6	1.4					4.3	3.1	3.2	2.0	5.6	4.9	3.8	3.6	4.3	2.3	4.2	3.8	0.09	0.14	0.19	0.18	0.18	0.28	0.17	0.34
38:1									2.8	2.6	2.3	1.7	0.7	1.1	0.8	1.2	0.2	0.3	0.4	0.4								
24:1					6.1	5.5	4.4	2.7																				
sum M	**8.4**	**6.7**	**5.3**	**3.9**	**6.1**	**5.5**	**4.4**	**2.7**	**8.2**	**6.5**	**6.3**	**4.5**	**6.8**	**6.8**	**5.1**	**5.6**	**5.2**	**3.9**	**5.7**	**6.0**	**0.3**	**0.6**	**0.5**	**0.7**	**0.2**	**0.4**	**0.2**	**0.3**
SD	1.4	0.7	0.8	0.8	0.6	0.6	0.8	0.5	0.8	1.3	0.9	1.4	0.3	1.8	2.0	1.0	0.8	0.8	1.3	2.0	0.1	0.2	0.3	0.2	0.1	0.1	0.1	0.2
sum S + M	**11.2**	**8.6**	**6.9**	**5.0**	**23.8**	**20.9**	**16.8**	**9.8**	**12.3**	**9.3**	**9.1**	**7.0**	**7.7**	**7.7**	**5.9**	**6.4**	**6.4**	**4.9**	**7.2**	**7.5**	**0.4**	**0.7**	**0.7**	**0.9**	**0.3**	**0.5**	**0.2**	**0.4**
SD	1.4	0.9	1.0	1.1	0.5	2.8	2.5	0.2	0.8	1.7	1.2	1.8	0.3	1.9	2.3	1.1	0.8	0.9	2.1	2.4	0.1	0.2	0.3	0.2	0.1	0.1	0.1	0.3
32:2	0.1	0.1	0.1	0.1																					0.02	0.05	0.02	0.02
32:3	0.3	0.5	0.6	0.6																								
34:2	0.5	0.5	0.4	0.3									0.1	0.2	0.2	0.2	0.1	0.2	0.2	0.3		0.16	0.15	0.15	0.02	0.12	0.02	0.05
34:3	0.4	0.7	0.8	0.9									0.1	0.1	0.2	0.2												
34:4	0.4	0.6	0.7	0.8									0.1	0.1	0.1	0.1												
34:5	0.2	0.2	0.2	0.2									0.1	0.2	0.2	0.3												
34:6													0.2	0.4	0.4	0.5												
36:2	1.7	1.5	1.0	1.0					0.9	1.1	0.6	0.4	0.6	0.6	0.5	0.5	1.9	1.0	1.8	1.8	0.05	0.09	0.11	0.11				
36:3	0.7	0.9	1.0	1.3					0.7	1.1	1.2	1.4	0.1	0.1	0.1	0.1												
36:4	1.7	3.0	3.2	4.5					0.6	0.7	0.8	1.0	0.2	0.2	0.2	0.2												
36:5	0.2	0.3	0.3	0.4									0.1	0.1	0.1	0.1												
38:2									1.0	0.9	0.8	0.8	0.6	1.0	0.6	0.9	0.9	0.9	1.4	1.5								
38:3									1.0	1.3	1.6	1.7	0.5	0.6	0.3	0.5	1.8	1.7	2.5	2.8								
38:4	1.0	1.4	1.6	2.1					1.9	2.9	3.5	4.6	0.2	0.3	0.2	0.2	2.3	2.6	3.1	3.4	0.03	0.06	0.04	0.06				
38:5	0.7	0.9	0.9	1.4					1.2	1.0	1.5	1.0	0.1	0.1	0.1	0.1	0.3	0.2	0.4	0.3	0.08	0.07	0.07	0.07				
38:6	0.2	0.2	0.2	0.3																	0.00	0.02	0.03	0.02				
40:3									1.6	0.7	0.8	1.4									0.07	0.22	0.08	0.10				
40:4	0.2	0.3	0.4	0.4					1.5	1.8	2.4	3.1					0.6	1.1	1.0	1.7	0.02	0.05	0.04	0.06				
40:5	0.2	0.3	0.5	0.4					0.9	1.0	0.9	1.3					1.0	1.5	1.5	2.7	0.05	0.09	0.09	0.14				
40:6	0.1	0.2	0.2	0.2									0.3	0.5	0.4	0.5	0.9	1.6	1.7	2.8	0.06	0.12	0.11	0.17				
40:7													0.2	0.3	0.6	0.3					0.12	0.21	0.20	0.34				
40:8													0.2	0.3	0.4	0.3												
42:5																					0.04	0.08	0.09	0.08				
42:6																					0.07	0.21	0.15	0.23				
42:7																					0.07	0.13	0.08	0.13				
18:2					0.4	0.5	0.7	0.7																				
18:3					1.2	1.7	2.5	2.5																				
20:2					0.7	1.0	1.3	1.5																				
20:3					1.5	2.3	3.4	3.5																				
sum P	**8.7**	**11.6**	**12.0**	**14.7**	**3.8**	**5.5**	**8.0**	**8.2**	**11.3**	**12.5**	**14.1**	**16.7**	**3.7**	**5.2**	**4.7**	**4.8**	**9.7**	**10.8**	**13.5**	**17.3**	**0.7**	**1.5**	**1.2**	**1.7**	**0.0**	**0.2**	**0.0**	**0.1**
SD	1.7	1.5	1.7	1.4	0.9	2.1	1.4	2.4	2.9	0.9	1.2	2.2	0.4	1.3	0.6	0.5	1.5	2.1	2.1	2.0	0.1	0.3	0.2	0.3	0.0	0.0	0.0	0.1
total	**19.9**	**20.2**	**18.9**	**19.7**	**27.6**	**26.4**	**24.8**	**18.0**	**23.6**	**21.8**	**23.1**	**23.7**	**11.5**	**12.8**	**10.6**	**11.2**	**16.0**	**15.7**	**20.7**	**24.9**	**1.1**	**2.2**	**1.9**	**2.5**	**0.3**	**0.6**	**0.2**	**0.5**
SD	2.7	2.3	2.7	2.1	1.0	3.6	3.5	2.6	3.3	2.0	2.4	2.7	0.4	3.2	2.4	0.6	2.1	2.8	3.9	4.4	0.1	0.3	0.5	0.4	0.1	0.1	0.1	0.3

[a]The *xx*:*y* notation denotes the total number of carbon atoms in the fatty acid chains (*xx*) and the number of double bonds (*y*). Standard deviations (SD) are given for the sums within each group. The data are averages over four measurements from a single representative experiment. sum S, sum M, and sum P are the sums of the saturated (S, db0), monounsaturated (M, db1), and polyunsaturated (P, db2−db4+) phospholipids (PL), respectively, where the degree of saturation refers to the number of double bonds in the fatty acid chains. The total PL composition for each time point is 100%. [b]Minutes stimulated with antigen.

Notable in these representative data is the high mol % of total SM in DRMs from unstimulated cells (27.6 mol % of the total phospholipids), indicative of highly purified DRM preparations, and similar to SM values of 20−23 mol % for DRM and nondetergent lipid raft preparations from KB cells characterized by Pike et al. (*28*). The mol % of SM decreases as a function of stimulation time, while the total level of PI increases with stimulation time as exemplified in Table 1. A compiled presentation of lipid compositional changes from many different experiments with DNP-BSA stimulation is shown in Figure 1A, where

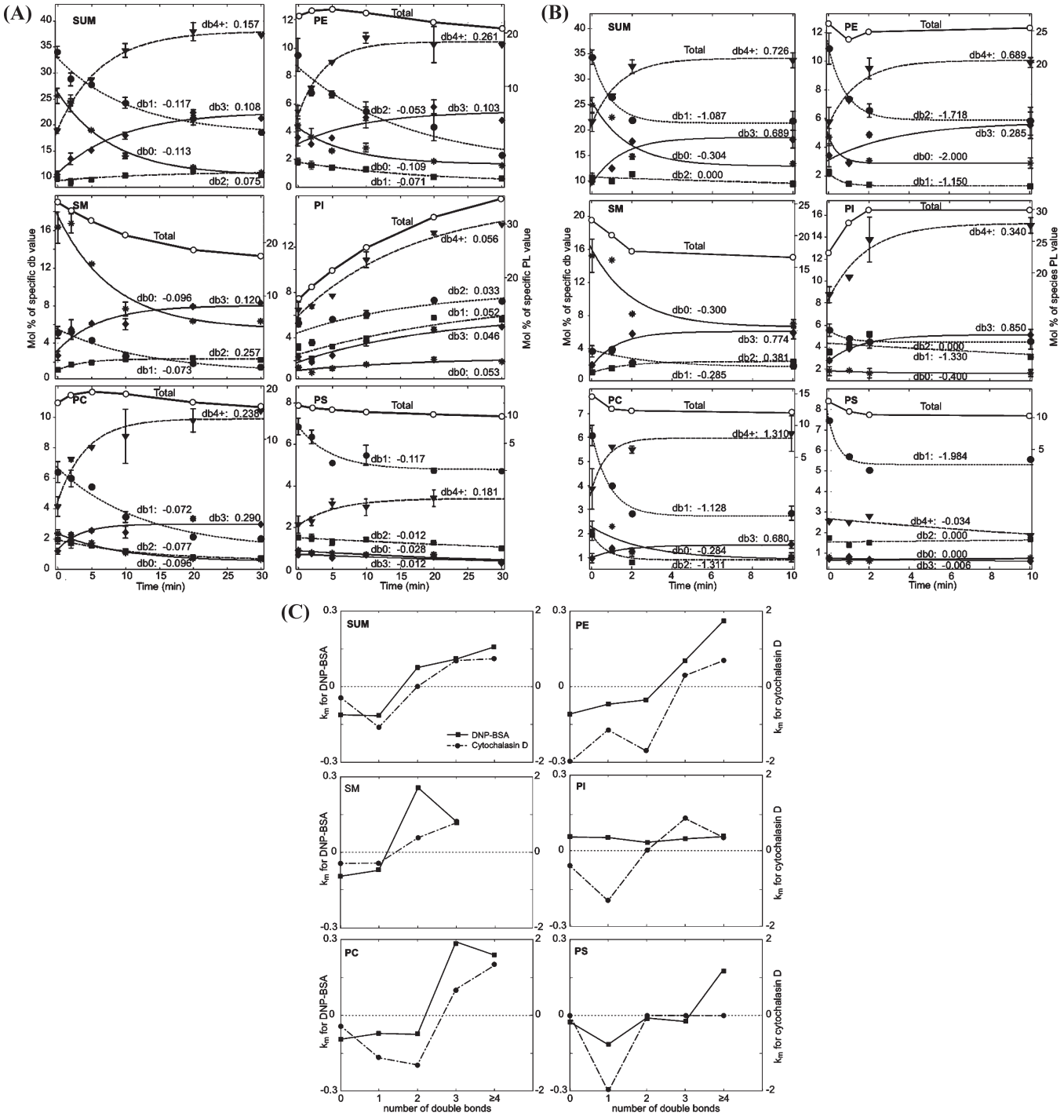

FIGURE 1: Mole percentages of phospholipids (PL) in DRMs that contain 0, 1, 2, 3, and ≥4 double bonds (db0, db1, db2, db3, and db4+, respectively) in the acyl chains vs (A) DNP-BSA antigen stimulation time (average of eight independent experiments) or (B) cytochalasin D stimulation time (average of four independent experiments) for each headgroup summed over headgroups. Data points corresponding to specified number of double bonds (each of db0, db1, db2, db3, and db4+) are fitted with an exponential decay corresponding to first-order kinetics (eq 1). Values of $k_m = nk$ (units of inverse minutes) are listed with each fitted curve. Errors bars show standard deviations from at least four separate experiments (0 and 10 min) or a range of values from two separate experiments (2, 5, and 20 min). Data points with no error bars represent a single experiment (1 and 30 min). (C) k_m values (units of inverse minutes) from panels A and B vs the number of double bonds for each headgroup for DNP-BSA stimulation (■, left ordinate) compared with cytochalasin D treatment (●, right ordinate).

the extensive data are represented in terms of headgroups (separate panels) and for each of these, the mol % of total PL (○, right ordinate). These compiled data show that, on average, the level of SM decreased from 28 to 17% after antigen stimulation for 30 min and the level of PI increased from 17 to 34% within this period; the other major PLs (PC, PE, and PS) show relatively small changes in total mol % as a function of stimulation time.

Lipid changes with respect to acyl chain unsaturation were evaluated (Figure 1A, black symbols, left ordinate). DNP-BSA stimulation time courses were measured in multiple experiments for stimulation times of typically 0, 2, 5, and 10 min, and in some experiments up to 20 and 30 min. We observe generally that the level of PL with more unsaturated acyl chains (more double bonds) tends to increase in the DRM fractions with stimulation time, whereas the levels of those with saturated or monounsatu-

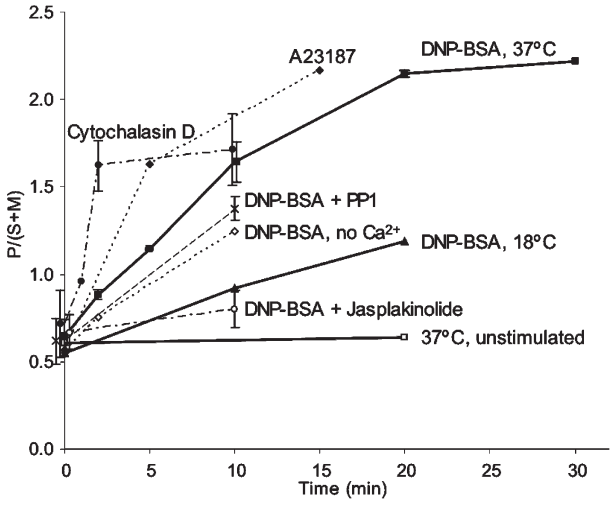

FIGURE 2: Ratio of polyunsaturated (P, db2−db4+) phospholipids to the sum of saturated (S, db0) and monounsaturated (M, db1) phospholipids [i.e., P/(S+M)] for the time course of stimulation by 5 μg/mL DNP-BSA at 37 °C (■, average of eight independent experiments) and 18 °C (▲), in the presence of 3 mM jasplakinolide (○, average of two independent experiments) or 4 μM PP1 (×, average of two independent experiments) or in the absence of media Ca^{2+} (◇) or by 2 μM cytochalasin D (●, average of four independent experiments) or 0.9 μM Ca^{2+} ionophore A23187 (◆). This ratio, P/(S+M), is also shown for DRMs from unstimulated cells incubated for 20 min at 37 °C prior to DRM preparation (□). Error bars show standard deviations from at least four separate experiments or a range from two separate experiments for each time point. Data points with no error bars represent only a single experiment with that time point.

rated acyl chains tend to decrease in these fractions. This is consistent with our previous observations made with DRMs derived from unstimulated cells and cells at a single (5 min) time point after DNP-BSA stimulation (*24*). That previous study compared the PL composition simply in terms of acyl chain saturation: saturated (S, 0 double bonds, db0), monounsaturated (M, 1 double bond, db1), and polyunsaturated (P, 2−4 or more double bonds, db2−db4+) and compiled the abundance data as the lumped ratio P/(S+M). This type of analysis of data in this study (Figure 2) showed that this simple ratio increases with cell stimulation. For stimulation by DNP-BSA at 37 °C (Figure 2, ■, thick line), the ratio increases approximately 4-fold with a half-time of ~7 min and stabilization by 20 min, whereas there are no changes over 20 min in the absence of stimulant (□, thick line). In comparison, DNP-BSA stimulation at 18 °C (▲, thick line) results in a somewhat slower, 2-fold increase in the P/(S+M) ratio by 20 min, consistent with the temperature dependence for other antigen-stimulated signaling processes in these cells (*34*). Stimulated cellular degranulation is not detectable at 18 °C (*34*), indicating that the lipid changes we observe at this temperature are not a consequence of degranulation.

We evaluated a first-order kinetic model (eq 1) for comprehensive evaluation of the detailed mol % data representing PL changes occurring in the DRM fractions after cell stimulation. Figure 1A shows first-order kinetic fits for data compiled from eight independent experiments with DNP-BSA stimulation. The data are fitted in terms of the total number of double bonds in the acyl chains (db0, db1, db2, db3, and db4+; left ordinate) associated with each headgroup (separate panels). (The minor species PG and PA, whose low mol % and corresponding large error bars result in more erratic behavior, are not shown.) Data accumulated over a 30 min stimulation are fitted with eq 1, which applies to species that undergo a decrease or increase in concentration. The quality of the fits shows that the compositional changes are consistent with a first-order kinetic model, and this analysis also provides a detailed accounting for our general observation that the degree of acyl chain unsaturation increases in DRM compartments after cells are stimulated with DNP-BSA (ref (*24*) and Figure 2).

With eq 1, the rate constants, k, for each number of double bonds within each headgroup can be determined from the exponential fits to the data (Figure 1A; black fit by eq 1, left ordinate). The lumped value $k_m = nk$ (where $n = 1$ or -1 for an increasing or decreasing concentration, respectively; see Materials and Methods) are listed with the respective curves in Figure 1A. These k_m values for DNP-BSA stimulation are plotted as a function of the number of double bonds for each headgroup species in Figure 1C (■). These plots summarize succinctly the dependence of stimulated DRM compositional changes on the degree of acyl chain unsaturation. Values of $k = |k_m|$ for each headgroup and for summed PLs are generally less than 0.3 min^{-1} for DNP-BSA stimulation (Figure 1C, left ordinate). It is notable in these plots that the x-axis is crossed as the k_m values go from negative (decreasing concentration) to positive (increasing concentration). For PC and PE, the k_m values go from negative to positive between two and three double bonds. For SM, with a single acyl chain, this change occurs between one and two double bonds. For PI, the concentration increases after DNP-BSA stimulation (positive k_m) for acyl chains with any number of double bonds. When the cumulative data are summed over all the lipid species (top left panel of Figure 1C), the transition from negative to positive k_m values occurs between one and two double bonds, justifying our choice of the ratio P/(S+M) in the simple data analysis used previously (ref (*24*) and Figure 2).

A linear approximation to eq 1, given by eq 2, was also used to evaluate data sets for DNP-BSA stimulation that were collected over shorter time periods (0−10 min). As an example, Figure 3 presents the data from the representative experiment in Table 1 in terms of the total number of double bonds in the acyl chains (db0, db1, db2, db3, and db4+) associated with each headgroup (PC, SM, PE, PI, PS, and sum) as a function of stimulation time (0, 2, 5, and 10 min). These data, fitted with eq 2, yield a slope corresponding to the apparent rate constant k_a times the direction and magnitude of the concentration change ($C_f - C_i$). These $k_s = (C_f - C_i)k_a$ values are listed with respective fitted lines in Figure 3. As expected from preceding analyses of cumulative data with eq 1 (Figure 1A,C), the k_s values for each PL headgroup tend to be more positive for a higher number of double bonds and more negative for a lower number of double bonds.

Figure 4 (■, thick line) plots the averaged $k_s = (C_f - C_i)k_a$ values from five independent experiments with DNP-BSA stimulation as a function of the number of double bonds for each headgroup species. As expected, these plots reveal the same trend as Figure 1C; i.e., there is a clear dependence of stimulated DRM compositional changes on the degree of acyl chain unsaturation, such that those with higher degrees of unsaturation increase after stimulation. We confirmed that results from eqs 1 and 2 show good agreement for short time periods (<10 min for DNP-BSA stimulation) as described in Materials and Methods. Therefore, we used the linear approximation (eq 2) to compare directly the DRM compositional changes caused by FcεRI-mediated activation with multiple other treatments, in many different experiments as described below (Figure 4).

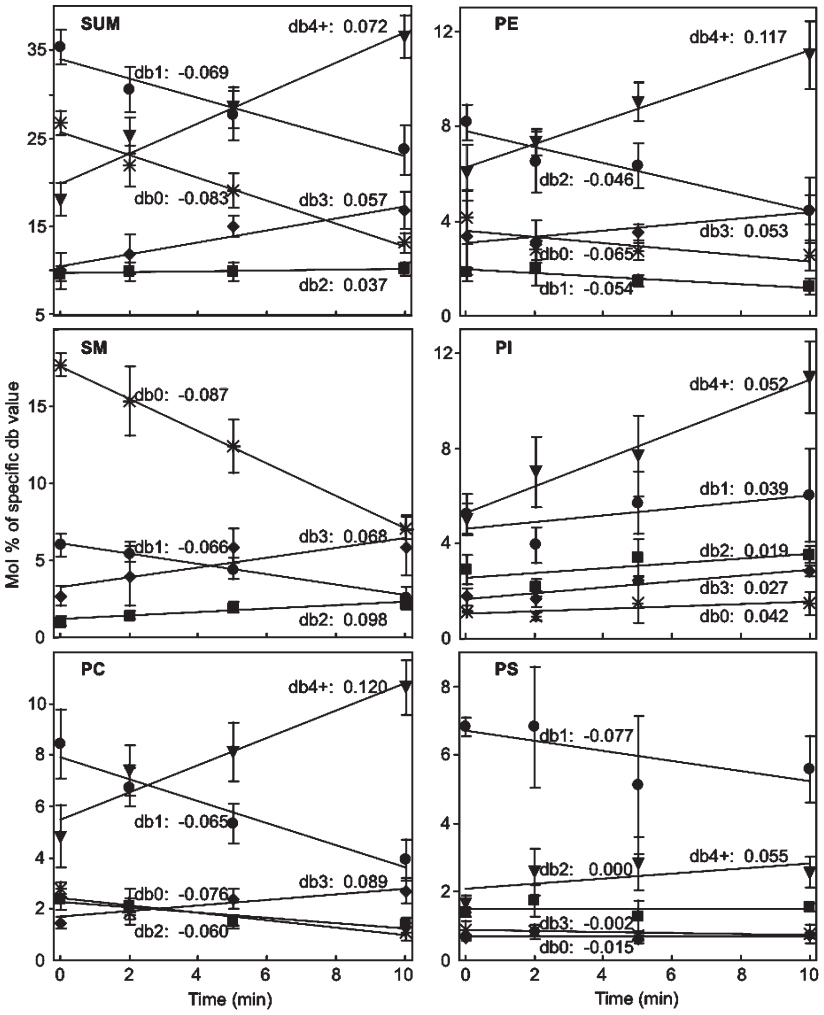

FIGURE 3: Representative data (Table 1) plotted as mol % of DRM phospholipids that contain 0, 1, 2, 3, and ≥4 double bonds (db0, db1, db2, db3, and db4+, respectively) in the acyl chains vs antigen stimulation time for each headgroup and summed over headgroups. Data points corresponding to each of db0, db1, db2, db3, and db4+ are fitted with a linear function corresponding to first-order kinetics at short times (eq 2). Values of $k_s = (C_f - C_i)k_a$ (units of mol %/min) are listed with each fitted curve. Error bars show the standard deviations from representative data in Table 1.

We considered alterations in the cholesterol levels or the total PL recovered as factors contributing to our consistent observation of substantial increases in the percentage of unsaturated PL in the DRM compartments after DNP-BSA stimulation. We previously showed under our current experimental conditions that cell lysis is complete and not significantly altered by stimulation (*16*, *18*, *59*). Furthermore, >80% of a GD_{1b} ganglioside marker is recovered in low-density DRM fractions under these conditions (*16*). In this study, we found that there is an ~20% increase in cholesterol content of the DRM following stimulation by antigen for 10 min at 37 °C, as determined with an enzymatic fluorescence assay for this sterol (Materials and Methods, data not shown). PL recovered in DRMs under the conditions used for their isolation in this study represent 11.2% + 2.6 (SD; n = 3) of cellular PL, based on organic phosphate analysis of chloroform-soluble PL extracted from DRMs and intact cells (see Materials and Methods). These DRMs contain PL from both plasma membrane and endocytic recycling compartments (N. Smith et al., unpublished results). To compare the relative amount of PL recovered in the DRM fraction before and after stimulation, a synthetic phospholipid standard, 1,2-dinonadecanoyl-*sn*-glycero-3-phosphatidylcholine, was added to each cell lysate sample at a concentration permitting its coquantification in ESI-MS analysis of the DRM fraction. As summarized in Table 2 (treatments 1 and 2), this analysis shows that DNP-BSA stimulation causes an ~40% molar increase in the level of PLs recovered in the DRM fraction relative to that for unstimulated cells. This is greater than the stimulated increase in DRM cholesterol, suggesting that the stimulated increase in polyunsaturated PLs recovered in DRMs is not due simply to changes in the cholesterol concentration in these compartments. Therefore, we investigated the involvement of other cellular components in the reorganization of DRM PLs caused by FcεRI-mediated cell activation.

Mechanistic Basis for Observed Changes. To probe the mechanism by which stimulation via FcεRI causes a marked change in the PL composition of DRMs, we examined the effect of the Src family kinase inhibitor, PP1, on these stimulated changes. As shown in the simple analysis of Figure 2 [P/(S+M) vs time], 4 μM PP1 has a weak effect on the DNP-BSA-stimulated response (×, dashed line). At the concentration evaluated, PP1 effectively inhibits most antigen-stimulated tyrosine phosphorylation detected in whole cell Western blots, although some FcεRI β and LAT phosphorylation persists (ref (*35*) and Figure S1 of the Supporting Information). The first-order kinetic analysis summarized in Figure 4 ($k_s = (C_f - C_i)k_a$ vs db#, based

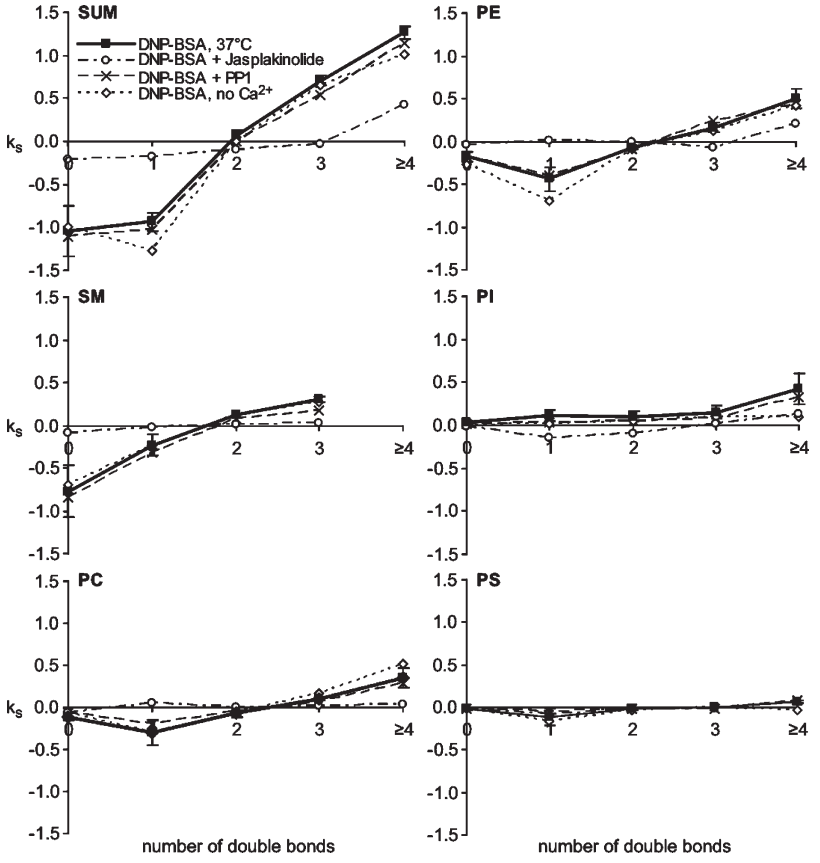

FIGURE 4: Values of $k_s = (C_f - C_i)k_a$ (eq 2; units of mol %/min) vs the number of double bonds in phospholipid fatty acid chains for DNP-BSA stimulation (average of five independent experiments; error bars show the standard deviation) compared with antigen stimulation in the presence of PP1, jasplakinolide, or Ca^{2+}-free medium (same treatments and number of experiments as in Figure 2).

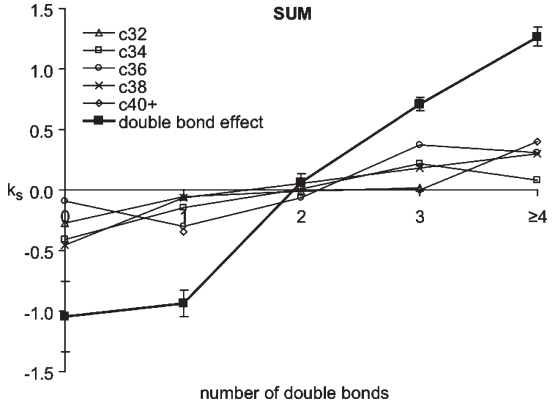

FIGURE 5: Representative data (Table 1) evaluated for cells stimulated with DNP-BSA and dependence of DRM phospholipid compositional changes on total acyl chain length. Values of $k_s = (C_f - C_i)$ k_a (eq 2, units of mol %/min) vs the number of double bonds are shown for separate chain lengths corresponding to 32, 34, 36, 38, and ≥40 carbons in both acyl chains (c32, c34, c36, c38, and c40+, respectively, summed over seven headgroups). The black squares and thick line correspond to k_s values vs the number of double bonds summed over all headgroups (double bond effect; duplicated from the top left panel of Figure 4).

Table 2: Comparison of Relative Recoveries of Phospholipids (PL) in DRMs Isolated after Specified Treatments of the Cells[a]

treatment	stimulant	inhibitor	ratio
1 (3)	none	none	1.00 ± 0.06
2 (3)	DNP-BSA	none	1.39 ± 0.11
3 (1)	none	PP1	0.90 ± 0.18
4 (1)	DNP-BSA	PP1	1.29 ± 0.09
5 (2)	cytochalasin D	none	1.29 ± 0.26
6 (1)	none	jasplakinolide	0.85 ± 0.12
7 (1)	DNP-BSA	jasplakinolide	0.95 ± 0.10

[a] The value in parentheses indicates the number of experiments for a specific treatment. The ratio is the relative amount of total DRM PL to an internal standard lipid (see Materials and Methods) under each condition. This ratio value is averaged from at least two experiments for treatments 1, 2, and 5 or from a single experiment for treatments 3, 4, 6, and 7 and normalized to treatment 1. Standard deviations are from multiple experiments or for single-experiment treatments were calculated from error propagation from standard deviations in four separate measurements.

on eq 2) shows that this concentration of PP1 present during antigen stimulation causes very little difference in PL compositional changes (compare ■ and ×). Table 2 (treatments 3 and 4) shows that this concentration of PP1 causes only a small change in the DNP-BSA-stimulated increase in recovery of PL in the DRM fraction. Together, these results suggest that the antigen-stimulated changes in PL composition of DRMs do not depend strongly on the tyrosine phosphorylation cascade that is initiated by FcεRI cross-linking.

Antigen stimulates a robust Ca^{2+} response in RBL mast cells, and this Ca^{2+} mobilization is necessary for degranulation (*34*, *35*). We investigated stimulated PL changes in DRMs caused by the Ca^{2+} ionophore A23187 that can stimulate RBL cell degranulation (in the absence of DNP-BSA). The simple analysis of Figure 2 shows that a stimulating dose of A23187 (0.9 μM) causes changes in PL composition very similar to those caused by DNP-BSA, but with faster kinetics (compare ◆ with ■). We also found that DNP-BSA stimulation of cells in buffer without extracellular Ca^{2+} (Figure 2, ◇) causes attenuation of the

antigen-stimulated increase in P/(S+M) but does not prevent it. Under these conditions, antigen stimulates a transient increase in the intracellular Ca^{2+} concentration without a sustaining influx of Ca^{2+} from the extracellular medium, which is insufficient in triggering degranulation (*36*, *37*). In the analysis of Figure 4, DNP-BSA stimulation in the absence of extracellular Ca^{2+} (◇) causes PL compositional changes similar to those caused by DNP-BSA in the presence of extracellular Ca^{2+} (■). These results show that a sustained increase in the intracellular Ca^{2+} concentration may contribute to, but is not necessary for, the antigen-stimulated changes in DRM lipid composition observed.

Role of the Cytoskeleton. Cytochalasin D disrupts the actin cytoskeleton by capping the barbed end of actin microfilaments and preventing elongation, thereby effectively preventing stimulated polymerization of F-actin (*38*). This inhibition of actin polymerization has been shown to enhance IgE receptor signaling in RBL mast cells (*38*, *39*). When testing whether cytochalasin D affects DNP-BSA-stimulated changes in DRM lipid composition, we were surprised to find that cytochalasin D alone causes similar changes, with faster kinetics, as indicated in Figure 2 (compare ● with ■). First-order kinetic analysis of cytochalasin effects provides detailed accounting of PL compositional changes according to headgroup and double bonds (Figure 1B). A summary of this analysis in terms of $k_m = nk$ values (eq 1) reveals that, compared with antigen stimulation (Figure 1C, ■, left ordinate), treatment of RBL cells with 2 μM cytochalasin D (Figure 1C, ●, right ordinate) causes significantly faster changes in DRM lipid composition for each headgroup: The k_m values are as much as 6-fold larger for cytochalasin D stimulation. Figure 1C also shows that the dependence of k_m values on the acyl chain unsaturation is similar to that of DNP-BSA for all the major PL headgroups, with some differences for PI. Latrunculin A is another inhibitor of actin polymerization that disrupts the actin cytoskeleton by a different mechanism: sequestration of monomeric G-actin to inhibit its incorporation into polymeric F-actin (*40*). Changes similar to those for 2 μM cytochalasin D (Figure 1C, ●) also occurred with 0.2 μM latrunculin A or with cytochalasin D at doses as low as 0.2 μM (data not shown). Only very small changes in net F-actin content occur under these conditions of cytochalasin D treatment (*38*), indicating that the DRM lipid composition is sensitive to relatively subtle changes in F-actin.

Overall, our results indicate that the mechanistic basis for the antigen-stimulated change in PL composition of DRMs may be stimulated depolymerization of cortical F-actin, which partially redistributes to other intracellular locations (*41*). To test this explanation, we examined the effect of jasplakinolide, which is known to stabilize F-actin (*42*), on antigen-stimulated changes in the PL composition of DRMs. We found that 3 μM jasplakinolide has no discernible effect on DRM composition in the absence of stimulation (Figure 2, ○ at 0 min). However, this reagent effectively inhibits the antigen-stimulated changes in PL composition as shown in Figure 2 (○ at 10 min) and in Figure 4 (○). Consistent with these observations, jasplakinolide inhibits the antigen-stimulated increase in the relative amount of PLs fractionating with DRMs (Table 2, treatments 1, 2, 6, and 7), whereas cytochalasin D causes PL increase similarly to antigen stimulation (Table 2, treatments 1, 2, and 5). Our results show that the actin cytoskeleton regulates the structural composition and stability of plasma membrane domains that fractionate as DRMs. Correspondingly, we conclude that antigen- and IgE receptor-mediated changes in the distribution of F-actin substantially modify the composition and/or stability during cell signaling of these membrane domains represented by the DRMs.

Dependence of DRM Compositional Change after Antigen Stimulation on the Length of Acyl Chains. Compositional changes in terms of acyl chain length associated with each headgroup were also evaluated after DNP-BSA stimulation with the first-order kinetic model. For this purpose, acyl chains associated with all headgroups were evaluated according to eq 2, in terms of both the combined length of their acyl chains and the total number of double bonds. These results are summarized for a single representative experiment (Table 1) in Figure 5, which compiles the chain length results for the major phospholipids PC, PE, and PI (SM with one rather than two acyl chains gave similar results). Compared on this same graph is the dependence of total DRM lipid compositional changes on the number of double bonds (■ and thick line reproduced from the top left panel in Figure 4). Whereas the dependence of lipid compositional change on the number double bonds is pronounced, as described above, there is negligible dependence on chain length.

DISCUSSION

Our detailed PL analysis in this study builds on previous observations to further our understanding of the interactions between lipid raft membrane domains and the actin cytoskeleton, and the regulation of these interactions by IgE receptor (FcεRI) signaling. Published studies on structural and functional roles for lipid rafts in cell biology number in the thousands, strongly implicating their critical participation in cellular homeostasis and stimulated responses, yet these compartments remain elusive to experimental definition because of their lipid and protein heterogeneity and their dynamic nature in living cells. Biochemical isolation of subcellular components is an essential part of structure−function analysis in live cells, even while recognizing that the procedures involved perturb their structures relative to those in live cells. Isolation of lipid rafts by detergent fractionation or other methods suffers the same pitfalls of this general approach, but it provides the necessary means for molecular characterization that can be further tested and refined in live cell experiments. DRM preparations have proven to be a useful correlative tool in elucidating the functional role of lipid rafts in FcεRI signaling (*8*).

We showed previously with ESI-MS that DRM preparations from RBL mast cells contain ~100 distinct PL species (*24*), highlighting the complexity that exists in these membranes. In the study presented here, we confirm and extend our initial observation that antigen cross-linking of IgE receptors stimulates changes in the PL composition of DRMs isolated before and after this cell activation. Furthermore, we discovered that this substantial compositional change depends on stimulated alterations in the actin cytoskeleton and appears largely independent of the tyrosine phosphorylation cascade that is activated in parallel to these cytoskeletal changes. This finding is surprising, as it indicates that the PL composition of detergent-resistant lipid rafts is much more sensitive to cytoskeletal regulation than to various phospholipases whose activation is stimulated by tyrosine phosphorylation (*43*, *44*). Consistent with this, only small changes in the total PL composition of RBL mast cells are detected due to antigen stimulation (*45*), indicating that net gain or loss of specific PL species due to stimulated PL turnover is likely to provide a relatively minor contribution to the large changes in DRM PL composition that we observe.

Our results implicate the actin cytoskeleton as strongly influencing the PL composition of DRM preparations. Relatively

small changes in net F-actin content caused by cytochalasin D or latrunculin A cause large and rapid changes in this composition, and antigen-stimulated changes are prevented by jasplakinolide. We observe net increases in the amount of PLs isolated as DRMs, and preferential increases in polyunsaturated lipids caused by inhibitors of F-actin polymerization or by antigen stimulation. These results suggest that interactions of the membrane with the actin cytoskeleton limit recovery of detergent-resistant lipids in resting cells and that cell stimulation or direct inhibition of F-actin polymerization weakens these interactions. Although antigen stimulation causes a net increase in the level of stimulated actin polymerization (*38*), it is possible that spatially localized actin depolymerization (*40*) is chiefly responsible for the increase in the level of detergent-resistant PL that are recovered under these conditions.

Our detailed kinetic analysis of extensive mass spectrometry data for DRMs provides a comprehensive means for investigating and comparing temporal changes in lipid composition that are initiated by various stimulants in the signaling pathway. This analysis compares the mol % content of individual lipid species within the total lipids collected in the isolated membranes, and thereby structural and physical changes that accompany specific cell stimulating conditions. In a previous study (*46*), Milne et al. described a lipid array study using ESI-MS coupled with computational approaches to identify the lipid pattern of total cellular lipids, and changes in the pattern as indicated by the relative change in peak abundance over the defined time course of antigen stimulation in B cells. Our kinetic study presents an effective way to characterize lipid compositional change in the context of functionally relevant membrane domains and pinpoints subtle changes related to specific stimulating conditions. Thus, our kinetic approach should be a valuable tool for lipidomic studies toward understanding membrane signaling.

Our ESI-MS analysis is conducted on DRMs isolated after cell lysis in a relatively low concentration of TX-100 (0.045%). These conditions were chosen because they discriminate between cross-linked and un-cross-linked IgE receptors as DRM components, whereas other components of lipid rafts, such as the GPI-anchored protein Thy-1, are efficiently recovered in DRMs in the presence or absence of IgE receptor cross-linking (*16*, *18*, *47*). It is possible that a different sensitivity to antigen stimulation or F-actin inhibitors would be observed at higher concentrations of detergent, but substantial detergent interference under these conditions precludes accurate mass spectrometric analysis of the PL composition (*24*). Special LiCl extraction conditions gave essentially the same results, with no indication of plasmalogen species at m/z 720.5, 722.5, 770.6, and 774.6 as reported by others (*28*, *48*, *49*). This may reflect differences in the membrane preparations or cell growth conditions. It is notable that cytochalasin D does not change the percent recovery of cross-linked IgE receptors with DRMs under the conditions of our experiments. However, this treatment does decrease the density of detergent-resistant FcεRI-containing membranes, as separated in sucrose gradients, consistent with cytoskeletal interactions by these detergent-resistant receptors in the absence of cytochalasin D (*21*).

The changes in DRM PL composition we observe are stimulated by the Ca^{2+} ionophore A23187 (Figure 2). They are also stimulated by antigen in the absence of extracellular Ca^{2+} (Figures 2 and 4), a condition that inhibits degranulation and most signaling processes downstream of FcεRI (*36*, *50*). Interestingly, activation of permeabilized mast cells by either micromolar Ca^{2+} or GTPγ-S in the presence of EGTA results in redistribution of F-actin from the periphery to the cell interior in a process that is similar to that stimulated in intact mast cells (*51*, *52*). These results suggest that redistribution of F-actin from the cell cortex can be elicited by both Ca^{2+}-dependent and Ca^{2+}-independent stimuli, and this may be relevant to the PL changes in DRM that we observe.

A model to explain our results is one in which loss of F-actin proximal to the plasma membrane caused by antigen activation or by inhibitors of actin polymerization perturbs the structural regulation of nanoscopic Ld/Lo-like phase separation. This could result in lipid redistributions that enhance the recovery of polyunsaturated PLs, particularly those with PI headgroups, in DRM fractions. Preferential interactions of polyphosphatidylinositol PLs with the actin cytoskeleton at the inner leaflet of the plasma membrane (*23*, *53*) may be relevant to this process, and the negative charge of PI may also contribute to these interactions. In this scenario, disruption of interactions between PI and structural proteins by antigen stimulation or by inhibitors of actin polymerization could result in an increased recovery of PI in detergent-resistant, low-density membranes. Future efforts are aimed at detecting in intact cells the membrane structural changes manifested by our ESI-MS analysis of DRM PLs. To this end, biophysical methods such as resonance energy transfer (*54*, *55*), fluorescence correlation spectroscopy (*56*), and electron spin resonance (*57*) are proving use to be useful approaches to studying membrane lipid heterogeneity in live cells.

SUPPORTING INFORMATION AVAILABLE

Western blot showing that PP1 inhibits tyrosine phosphorylation that is stimulated by antigen DNP-BSA in RBL-2H3 mast cells sensitized with anti-DNP IgE (Figure S1). This material is available free of charge via the Internet at http://pubs.acs.org.

REFERENCES

(1) Mukherjee, S., and Maxfield, F. R. (2004) Membrane domains. *Annu. Rev. Cell Dev. Biol. 20*, 839–866.
(2) Brown, D. A. (2005) Lipid Rafts: From Model Membranes to Cells. *Biochim. Biophys. Acta 1746*, 182–195.
(3) Simons, K., and Toomre, D. (2000) Lipid rafts and signal transduction. *Nat. Rev. Mol. Cell Biol. 1*, 31–39.
(4) Brown, D. A., and Rose, J. K. (1992) Sorting of GPI-anchored proteins to glycolipid-enriched membrane subdomains during transport to the apical cell surface. *Cell 68*, 533–544.
(5) Cinek, T., and Horejsi, V. (1992) The nature of large noncovalent complexes containing glycosyl-phosphatidylinositol-anchored membrane glycoproteins and protein tyrosine kinases. *J. Immunol. 149*, 2262–2270.
(6) Simons, K., and Ikonen, E. (1997) Functional rafts in cell membranes. *Nature 387*, 569–572.
(7) Anderson, R. G. (1998) The caveolae membrane system. *Annu. Rev. Biochem. 67*, 199–225.
(8) Holowka, D., Gosse, J. A., Hammond, A. T., Han, X., Sengupta, P., Smith, N. L., Wagenknecht-Wiesner, A., Wu, M., Young, R. M., and Baird, B. (2005) Lipid segregation and IgE receptor signaling: A decade of progress. *Biochim. Biophys. Acta 1746*, 252–259.
(9) Smith, A. E., and Helenius, A. (2004) How viruses enter animal cells. *Science 304*, 237–242.
(10) Munro, S. (2003) Lipid rafts: Elusive or illusive?. *Cell 115*, 377–388.
(11) Edidin, M. (2003) The state of lipid rafts: From model membranes to cells. *Annu. Rev. Biophys. Biomol. Struct. 32*, 257–283.
(12) Sengupta, P., Baird, B., and Holowka, D. (2007) Lipid rafts, fluid/fluid phase separation, and their relevance to plasma membrane structure and function. *Semin. Cell Dev. Biol. 18*, 583–590.
(13) Brown, D. A. (2006) Lipid rafts, detergent-resistant membranes, and raft targeting signals. *Physiology 21*, 430–439.
(14) Janes, P. W., Ley, S. C., and Magee, A. I. (1999) Aggregation of lipid rafts accompanies signaling via the T cell antigen receptor. *J. Cell Biol. 147*, 447–461.

(15) Harder, T., Scheiffele, P., Verkade, P., and Simons, K. (1998) Lipid domain structure of the plasma membrane revealed by patching of membrane components. *J. Cell Biol. 141*, 929–942.

(16) Sheets, E. D., Holowka, D., and Baird, B. (1999) Critical role for cholesterol in Lyn-mediated tyrosine phosphorylation of FcεRI and their association with detergent-resistant membranes. *J. Cell Biol. 145*, 877–887.

(17) Pyenta, P. S., Holowka, D., and Baird, B. (2001) Cross-correlation analysis of inner-leaflet-anchored green fluorescent protein co-redistributed with IgE receptors and outer leaflet lipid raft components. *Biophys. J. 80*, 2120–2132.

(18) Field, K. A., Holowka, D., and Baird, B. (1997) Compartmentalized activation of the high affinity immunoglobulin E receptor with membrane domains. *J. Biol. Chem. 272*, 4276–4280.

(19) Gosse, J. A., Wagenknecht-Wiesner, A., Holowka, D., and Baird, B. (2005) Transmembrane sequences are determinants of immunoreceptor signaling. *J. Immunol. 175*, 2123–2131.

(20) Harder, T., and Simons, K. (1999) Clusters of glycolipid and glycosylphosphatidylinositol-anchored proteins in lymphoid cells: Accumulation of actin regulated by local tyrosine phosporylation. *Eur. J. Immunol. 29*, 556–562.

(21) Holowka, D., Sheets, E. D., and Baird, B. (2000) Interactions between Fc(ε)RI and lipid raft components are regulated by the actin cytoskeleton. *J. Cell Sci. 113*, 1009–1019.

(22) Wu, M., Holowka, D., Craighead, H. G., and Baird, B. (2004) Visualization of plasma membrane compartmentalization with patterned lipid bilayers. *Proc. Natl. Acad. Sci. U.S.A. 101*, 13798–13803.

(23) Kwik, J., Boyle, S., Fooksman, D., Margolis, L., Sheetz, M. P., and Edidin, M. (2003) Membrane cholesterol, lateral mobility, and the phosphatidylinositol 4,5-bisphosphate-dependent organization of cell actin. *Proc. Natl. Acad. Sci. U.S.A. 100*, 13964–13969.

(24) Fridriksson, E. K., Shipkova, P. A., Sheets, E. D., Holowka, D., Baird, B., and McLafferty, F. W. (1999) Quantitative analysis of phospholipids in functionally important membrane domains from RBL-2H3 mast cells using tandem high-resolution mass spectrometry. *Biochemistry 38*, 8056–8063.

(25) Barsumian, E. L., Isersky, C., Petrino, M. G., and Siraganian, R. P. (1981) IgE-induced histamine release from rat basophilic leukemia cell lines: Isolation of releasing and nonreleasing clones. *Eur. J. Immunol. 11*, 317–323.

(26) Posner, R. G., Lee, B., Conrad, D. H., Holowka, D., Baird, B., and Goldstein, B. (1992) Aggregation of IgE-receptor complexes on rat basophilic leukemia cells does not change the intrinsic affinity but can alter the kinetics of the ligand-IgE interaction. *Biochemistry 31*, 5350–5356.

(27) Bligh, E. G., and Dyer, W. J. (1959) A rapid method of total lipid extraction and purification. *Can. J. Biochem. Physiol. 37*, 911–917.

(28) Pike, L. J., Han, X., Chung, K., and Gross, R. W. (2002) Lipid rafts are enriched in arachidonic acid and plasmenylethanolamine and their composition is independent of caveolin-1 expression: A quantitative electrospray ionization/mass spectrometric analysis. *Biochemistry 41*, 2075–2088.

(29) Beu, S. C., Senko, M. W., Quinn, J. P., Wampler, F. M., and McLafferty, F. W. (1993) Fourier-transform electrospray instrumentation for tandem high-resolution mass spectrometry of large molecules. *J. Am. Soc. Mass Spectrom. 4*, 557–565.

(30) Wilm, M. S., and Mann, M. (1994) Electrospray and Taylor-Cone theory, Dole's beam of macromolecules at last?. *Int. J. Mass Spectrom. Ion Processes 136*, 176–180.

(31) Wilm, M. S., and Mann, M. (1996) Analytical properties of the nanoelectrospray ion source. *Anal. Chem. 68*, 1–8.

(32) Kim, H.-Y., Wang, T. C. L., and Ma, Y. C. (1994) Liquid chromatography/mass spectrometry of phospholipids using electrospray ionization. *Anal. Chem. 66*, 3977–3982.

(33) Han, X., and Gross, R. W. (1994) Electrospray ionization mass spectroscopic analysis of human erythrocyte plasma membrane phospholipids. *Proc. Natl. Acad. Sci. U.S.A. 91*, 10635–10639.

(34) WoldeMussie, E., Maeyama, K., and Beaven, M. A. (1986) Loss of secretory response of rate basophilic leukemia (2H3) cells at 40 °C is associated with reversible supression of inositol phospholipid breakdown and calcium signals. *J. Immunol. 137*, 1674–1680.

(35) Amoui, M., Draber, P., and Draberova, L. (1997) Src family-selective tyrosine kinase inhibitor, PP1, inhibits both FcεRI- and Thy-1-mediated activation of rat basophilic leukemia cells. *Eur. J. Immunol. 27*, 1881–1886.

(36) Beaven, M. A., Rogers, J., Moore, J. P., Hesketh, T. R., Smith, G. A., and Metcalfe, J. C. (1984) The mechanism of the calcium signal and correlation with histamine release in 2H3 cells. *J. Biol. Chem. 259*, 7129–7136.

(37) Mohr, F. C., and Fewtrell, C. (1987) Depolarization of rat basophilic leukemia cells inhibits calcium uptake and exocytosis. *J. Cell Biol. 104*, 783–792.

(38) Frigeri, L., and Apgar, J. R. (1999) The role of actin microfilaments in the down-regulation of the degranultion response in RBL-2H3 mast cells. *J. Immunol. 162*, 2243–2250.

(39) Narasimhan, V., Holowka, D., and Baird, B. (1990) Microfilaments regulate the rate of exocytosis in rat basophilic leukemia cells. *Biochem. Biophys. Res. Commun. 171*, 222–229.

(40) Coue, M., Brenner, S. L., Spector, I., and Korn, E. D. (1987) Inhibition of actin polymerization by latrunculin A. *FEBS Lett. 213*, 316.

(41) Koffer, A., Tatham, P. E., and Gomperts, B. D. (1990) Changes in the state of actin during the exocytotic reaction of permeabilized rat mast cells. *J. Cell Biol. 111*, 919–927.

(42) Bubb, M. R., Spector, I., Beyer, B. B., and Fosen, K. M. (2000) Effects of jasplakinolide on the kinetics of actin polymerization. An explanation for certain in vivo observations. *J. Biol. Chem. 275*, 5163–5170.

(43) Beaven, M. A., and Metzger, H. (1993) Signal transduction by Fc receptors: The FcεRI case. *Immunol. Today 14*, 222–226.

(44) Field, K. A., Apgar, J. R., Hong-Geller, E., Siraganian, R. P., Baird, B., and Holowka, D. (2000) Mutant RBL mast cells defective in FcεRI signaling and lipid raft biosynthesis are reconstituted by activated Rho-family GTPases. *Mol. Biol. Cell 11*, 3661–3673.

(45) Cohen, J. S. (2001) The role of phospholipid metabolism in regulated secretion in RBL mast cells. Ph.D. Thesis, Cornell University, Ithaca, NY.

(46) Milne, S. B., Forrester, P. T., Ivanova, P. T., Armstrong, M. D., and Brown, H. A. (2003) Multiplexed lipid arrays of anti-immunoglobulin M-induced changes in the glycerophospholipid composition of WEHI-231 cells. AfCS Reports (www.signaling-gateway.org/reports/vl/DA0011/DA0011.htm), Oct. 24, Vol. 11.

(47) Field, K. A., Holowka, D., and Baird, B. (1995) FcεRI-mediated recruitment of p53/56lyn to detergent-resistant membrane domains accompanies cellular signaling. *Proc. Natl. Acad. Sci. U.S.A. 92*, 9201–9205.

(48) Pike, L. J., Han, X., and Gross, R. W. (2005) Epidermal growth factor receptors are localized to lipid rafts that contain a balance of inner and outer leaflet lipids. *J. Biol. Chem. 280*, 26796–26804.

(49) Surviladze, Z., Harrison, K. A., Murphy, R. C., and Wilson, B. S. (2007) FcεRI and Thy-1 domains have unique protein and lipid compositions. *J. Lipid Res. 48*, 1325–1335.

(50) Beaven, M. A., and Ludowyke, R. (1989) Stimulatory signals for secretion in mast cells and basophils. In Advances in Regulation of Cell Growth , pp 245−285, Raven Press, New York.

(51) Norman, J. C., Price, L. S., Ridley, A. J., Hall, A., and Koffer, A. (1994) Actin filament organization in activated mast cells is regulated by heterotrimeric and small GTP-binding proteins. *J. Cell Biol. 126*, 1005–1015.

(52) Ludowyke, R. I., Kawasugi, K., and French, P. W. (1994) PMA and calcium ionophore induce myosin and F-actin rearrangement during histamine secretion from RBL-2H3 cells. *Cell Motil. Cytoskeleton 29*, 354–365.

(53) Raucher, D., Stauffer, T., Chen, W., Shen, K., Guo, S., York, J. D., Sheetz, M. P., and Meyer, T. (2000) Phosphatidylinositol 4,5-bisphosphate functions as a second messenger that regulates cytoskeleton-plasma membrane adhesion. *Cell 100*, 221–228.

(54) Zacharias, D. A., Violin, J. D., Newton, A. C., and Tsien, R. Y. (2002) Partitioning of lipid-modified monomeric GFPs into membrane microdomains of live cells. *Science 296*, 913–916.

(55) Sengupta, P., Holowka, D., and Baird, B. (2007) Fluorescence Resonance Energy Transfer Between Lipid Probes Detects Nanoscopic Heterogeneity in the Plasma Membrane of Live Cells. *Biophys. J. 92*, 3564–3574.

(56) Bacia, K., Scherfeld, D., Kahya, N., and Schwille, P. (2004) Fluorescence correlation spectroscopy relates rafts in model and native membranes. *Biophys. J. 87*, 1034–1043.

(57) Swamy, M. J., Ciani, L., Ge, M., Smith, A. K., Holowka, D., Baird, B., and Freed, J. H. (2006) Coexisting domains in the plasma membranes of live cells characterized by spin-label ESR spectroscopy. *Biophys. J. 90*, 4452–4465.

(58) Kingsley, P. B., and Feigenson, G. W. (1979) The synthesis of a perdeuterated phospholipid: 1,2-Dimyristoyl-*sn*-glycero-3-phosphocholine-d_{72}. *Chem. Phys. Lipids 24*, 135–147.

(59) Field, K. A., Holowka, D., and Baird, B. (1999) Structural aspects of the association of FcεRI with detergent resistant membranes. *J. Biol. Chem. 274*, 1753–1758.